ELSEVIER

Journal of Structural Geology 28 (2006) 669–681

JOURNAL OF STRUCTURAL GEOLOGY

www.elsevier.com/locate/jsg

Variations in fracture aperture above normal faults: a numerical investigation in 2-D elastic multilayers

Ghislain de Joussineau *, Jean-Pierre Petit

Laboratoire de Dynamique de la Lithosphère (UMR 5573), c.c. 060, Université Montpellier II, Place Eugène Bataillon, 34095 Montpellier, cedex 5, France

Received 2 April 2005; received in revised form 30 January 2006; accepted 31 January 2006
Available online 20 March 2006

Abstract

This work is a 2D numerical contribution to the problem of fault and fracture interaction in layered rocks, focusing on fracture aperture. We investigate the influence of an underlying normal fault on the aperture of open fractures in bonded multilayers submitted to vertical shortening and horizontal lengthening. The tests are carried out using the finite element code Franc 2D under plane strain conditions. It is first shown that the presence of a straight normal fault affects the aperture of the above fractures. The fractures located in two very local areas near the upper tip of the fault, one in the hanging wall and one in the footwall, tend to open, whereas the neighboring fractures tend to close. The increases in aperture are systematically greater in the footwall than in the hanging wall. Furthermore, the two areas with increased fracture aperture move towards the footwall when the dip of the fault increases. Second, the case of more complex underlying faults with restraining/releasing bends is studied. These models have similar results to those observed in the case of the straight underlying fault, with two areas of increased fracture aperture. The increases in fracture aperture are comparable with the case of the straight fault in the hanging wall, but are larger in the footwall. The contrasting behaviors of fractures described in the experiments are interpreted as a consequence of changes in the stress field in the central fractured layer caused by the presence of the underlying fault. They may provide a guide to explain fluid flow in fault tip areas. Finally, the case of fracture corridors (swarms of closely spaced fractures) is addressed. It is shown that, whatever the characteristics of the underlying fault, the total aperture of a corridor formed by three equally spaced fractures is equal to 1.41–1.69 times the aperture of a single fracture located at the same place in the fractured layer. This strongly suggests that these structures may act as preferential geological drains, with important consequences in terms of fluid flow.

Keywords: Elastic multilayer; Fracture aperture; Fracture corridor; Fluid flow; Fault tip; Franc 2D

1. Introduction

Faults and small (bed limited, i.e. layer-bound) fractures are very common geological structures coexisting in layered rocks in subsurface conditions. They may be linked physically to each other, for example when fractures develop as mode I branches in the extensional quadrant at the tips of sheared faults (Petit and Barquins, 1988). Slight displacements along faults can also have an important influence on the aperture of small and pervasive background fractures located at the fault proximity by modifying the local elastic stress field. These fracture apertures are of practical importance as they directly control flow, as shown by Fig. 1. In this field example of an exhumed palaeo oil reservoir in Abruzzo (Central Italy), the fractures and rock pores located in the brecciated hanging wall of a normal fault are open and exhibit oil flow, whereas fractures and pores in the footwall are closed to fluid circulation. This outcrop highlights the crucial impact of the deformation and stress around faults on flow through neighboring fractures. But while the role of fractures as geological conduits has been recognized and widely studied during the two past decades (Oda, 1986; Pyrak-Nolte et al., 1988; Cacas et al., 1990; Nordqvist et al., 1992; Gringarten, 1996; Bai and Pollard, 2001), and faulting has been recognized to influence fluid flow in rocks (Antonellini and Aydin, 1994; Aydin, 2000; Eichhulb et al., 2004), to our knowledge no work focusing specifically on the mechanical and flow capacity response of fractures due to the presence of an unconnected underlying normal fault has been published. Thus, several fundamental questions remain:

* Corresponding author. Now at: Department of Geological and Environmental Sciences, Stanford University, Stanford CA 94305, USA. Tel.: +1 650 723 4788; fax: +1 650 725 0979.
E-mail address: dejoussi@stanford.edu (G. de Joussineau).

0191-8141/$ - see front matter © 2006 Elsevier Ltd. All rights reserved.
doi:10.1016/j.jsg.2006.01.011

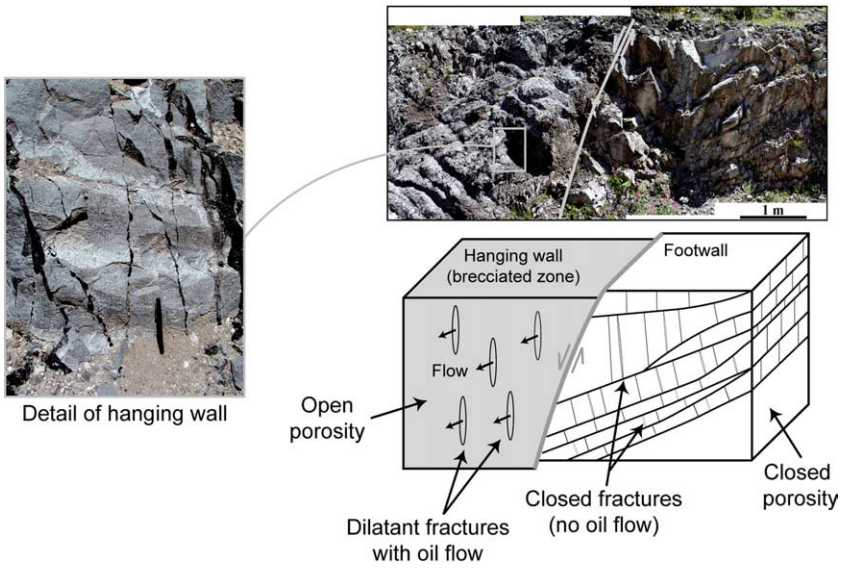

Fig. 1. Photographs and interpretation of an outcrop in the Lettomanopello quarry (Majella mountain, Central Italy): the normal fault separates an 'intact' compartment (footwall on the right part of the outcrop, where no oil circulation occurs through fractures) and a highly dilatant brecciated compartment characterized by oil flow through rock pores and fractures (hanging wall, left part of the outcrop: the scale of the detailed photograph is given by the pen).

- How do open fractures behave in response to stress perturbations near the tip of an underlying normal fault? Do they tend to open or to close? Does their behavior depend on their location with respect to the fault?
- What are the possible changes in fracture aperture that can be expected above a normal fault?
- Is the behavior of fractures influenced by the dip/geometry of the underlying fault? Do complex geometries of releasing/restraining bends lead to fracture behaviors different from the case of a straight fault?

In this paper, we propose possible answers to these questions, based on a 2D numerical approach in fractured elastic multilayers. In the experiments carried out, we considered neither fracture roughness, which can be of the same order as the fracture aperture (Renshaw, 1995), nor sealing phenomenon, in order to focus on the mechanical consequence of the presence of a normal fault on the aperture of fractures above. We used the code Franc 2D (Wawrzynek and Ingraffea, 1987), whose ability to accurately model fracture apertures has been demonstrated (Bai et al., 2000b; Bai and Pollard, 2001). The fracture aperture was approximated as a normal-displacement discontinuity as in Bai and Pollard (2001). In a first stage, we address the problem of a straight underlying fault with varying dip, and in a second stage, we investigate more complex geometries of releasing/restraining bends. Finally, we consider the case of fracture corridors (swarms of closely spaced sub-parallel mode I fractures horizontally and vertically persistent in a thick mechanical unit), which have been described in many geological environments (Connolly, 1999; Petit et al., 2004) and may act as preferential geological drains for fluids. We estimate the increase in aperture due to the presence of fracture corridors formed by three closely spaced fractures by comparing the total aperture in the corridors with the aperture of single fractures located in the same place in the models, for several fault configurations.

2. Numerical procedure

In this study, we use the code Franc 2D (Wawrzynek and Ingraffea, 1987), which permits the computation of stress fields in multilayer models (Fisher et al., 1995; Gross et al., 1995; Bai and Pollard, 2000a,b; Bai et al., 2000a; Engelder and Peacock, 2001; McConaughy and Engelder, 2001), the accurate evaluation of stress intensity factors and energy release rates at fracture tips (Bai and Pollard, 2000b; de Joussineau, 2003a,b), and most important to this study, precise predictions of fracture apertures (Bai et al., 2000b; Bai and Pollard, 2001).

This code is a 2D Finite Element code allowing one to study the deformation of elastic and elastoplastic models. It can solve linear or non-linear problems and, in this study, all our models were analyzed using a linear elastic method.

The models presented contain five bonded layers with common Poisson's ratio $v1 = v2$ equal to 0.3 (comparable with that of sedimentary rocks), and contrasting Young moduli (Fig. 2a): the stiff layers have a Young modulus E1 equal to 30 GPa (modulus of a limestone; Atkinson, 1987) and the soft layers have a Young modulus E2 equal to 3 GPa (modulus of a marl; Atkinson, 1987). We chose not to vary the Poisson's ratio between the layers in the models because this parameter varies far less than the Young modulus in consolidated sedimentary rocks. The Young moduli chosen fall into the wide range of Young moduli measured in sedimentary rocks (varying from 0.125 to 103 GPa; Bai and Pollard, 2000a). They correspond to intact rocks, because in this study we do not take into account the effects of alteration/weathering around fractures, which may modify the mechanical properties of rocks and induce important variations in the Young moduli of the layers.

Thirteen open fractures are introduced in the central fractured layer, with a regular spacing equal to the height of the fractured layer (Fig. 2a). The initial aperture of the

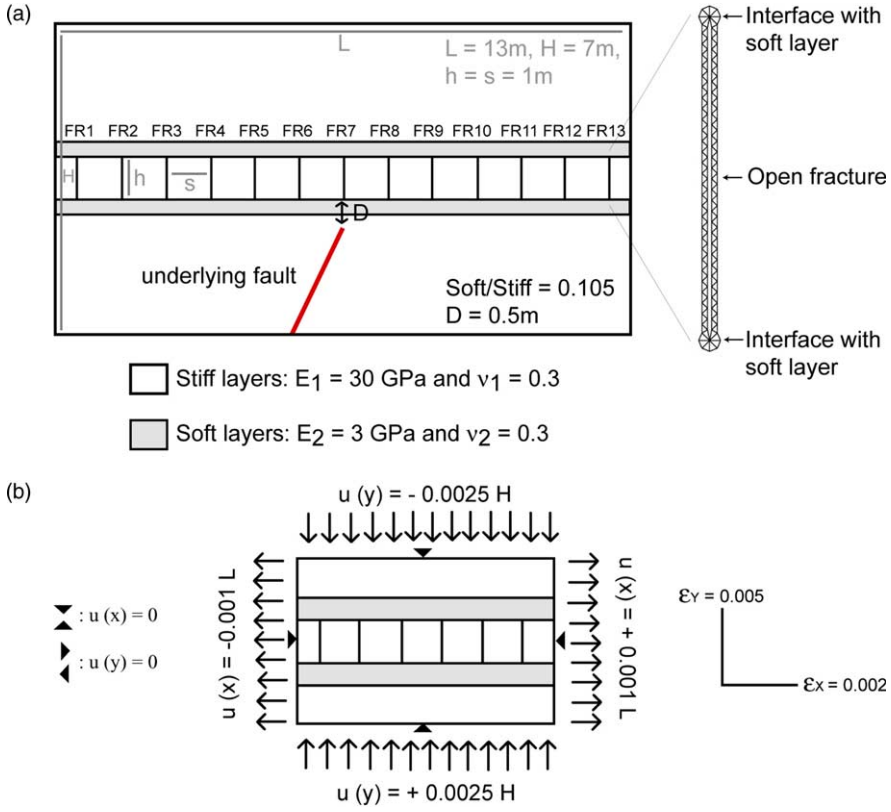

Fig. 2. (a) Geometry and characteristics of the models and mesh of the open fractures (indicated by symbols FR1–FR13, same convention used in following figures). (b) Boundary conditions applied to the models.

fractures, which is a condition of the numerical code used, is small (a few millimeters if the dimensions of the models are meters). A frictionless discontinuity is created in the bottom layer of the models, hereafter referred to as the *underlying fault*. Its upper tip lies under the thin soft layer (Fig. 2a).

The dimensions of the models have been determined by preliminary tests to have no influence on fracture apertures: models two times longer or two times higher in the part containing the underlying fault led to results similar to those described hereafter. The effect of the mesh on fracture aperture was also carefully tested, and the mesh used was built in order to have no influence on the numerical solution. In particular, the mesh was refined step by step around the fractures until calculated fracture apertures differed by less than 0.25% in two consecutive steps.

We impose displacement boundary conditions that result in a plane strain. The boundary conditions consist of both a vertical shortening (in the Y direction) equal to $2u_{(y)}/H = 0.005$, and a horizontal lengthening (in the X direction) equal to $2u_{(x)}/L = 0.002$ (Fig. 2b). These boundary conditions are applied to the models so that the underlying fault exhibits a normal displacement.

3. Results

In the experiments, the fracture aperture is approximated as a normal-displacement discontinuity, and is always measured in the middle of the fracture because the displacement discontinuity is known to vary along the surfaces of natural fractures (Pollard and Segall, 1987). The apertures are calculated as in Bai and Pollard (2001): $\delta = u_x(\mathrm{B}) - u_x(\mathrm{A})$, where δ is the fracture aperture, $u_x(\mathrm{B})$ is the horizontal displacement measured in B and $u_x(\mathrm{A})$ is the horizontal displacement measured in A (Fig. 3). The apertures of fractures FR1 and FR13 are not considered in the study because their position near the boundaries of the models perturbs their behavior (Bai et al., 2000b).

3.1. Straight underlying faults

In a first step, we examine the case of a straight underlying normal fault whose dip ranges from 50 to 80°. In the following, the fracture apertures are normalized to (divided by) the

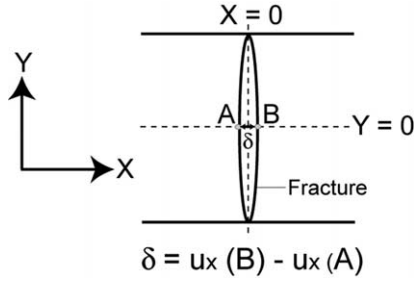

Fig. 3. Calculation of the fracture aperture δ as a normal-displacement discontinuity.

apertures of the same fractures calculated in a case with no underlying fault: normalized apertures greater than 1 indicate that the presence of the fault leads to an increase in fracture aperture and conversely, normalized apertures smaller than 1 indicate a decrease in aperture.

3.1.1. Hanging wall

Fig. 4a presents the normalized apertures of fractures FR2 to FR6 localized in the hanging wall of the fault; this figure shows that the tendencies in terms of fracture aperture vary greatly between the fractures depending on their position with respect to the underlying fault. Fractures FR2 and FR3 behave similarly: they exhibit an increase in aperture when the fault dips 50° (where the aperture of fracture FR3 is nearly multiplied by 2 with respect to the case without fault) but close severely when the fault dip is equal to or greater than 60°. Fracture FR4 presents a systematic increase in aperture with the presence of the underlying fault, but its normalized aperture is divided by almost 2 when the fault dip increases from 60° to 80°. Fracture FR5 behaves oppositely to fracture FR4: it closes when the fault dips 50°, but for larger fault dips it exhibits an increase in aperture that rises significantly when the fault dip increases from 60° to 70°. Finally, fracture FR6 closes when the fault dips 70° or less but opens slightly to strongly when the fault dip is 80° and 90°.

Fig. 4b summarizes these tendencies by showing the location of the area of increased fracture aperture in the hanging wall:

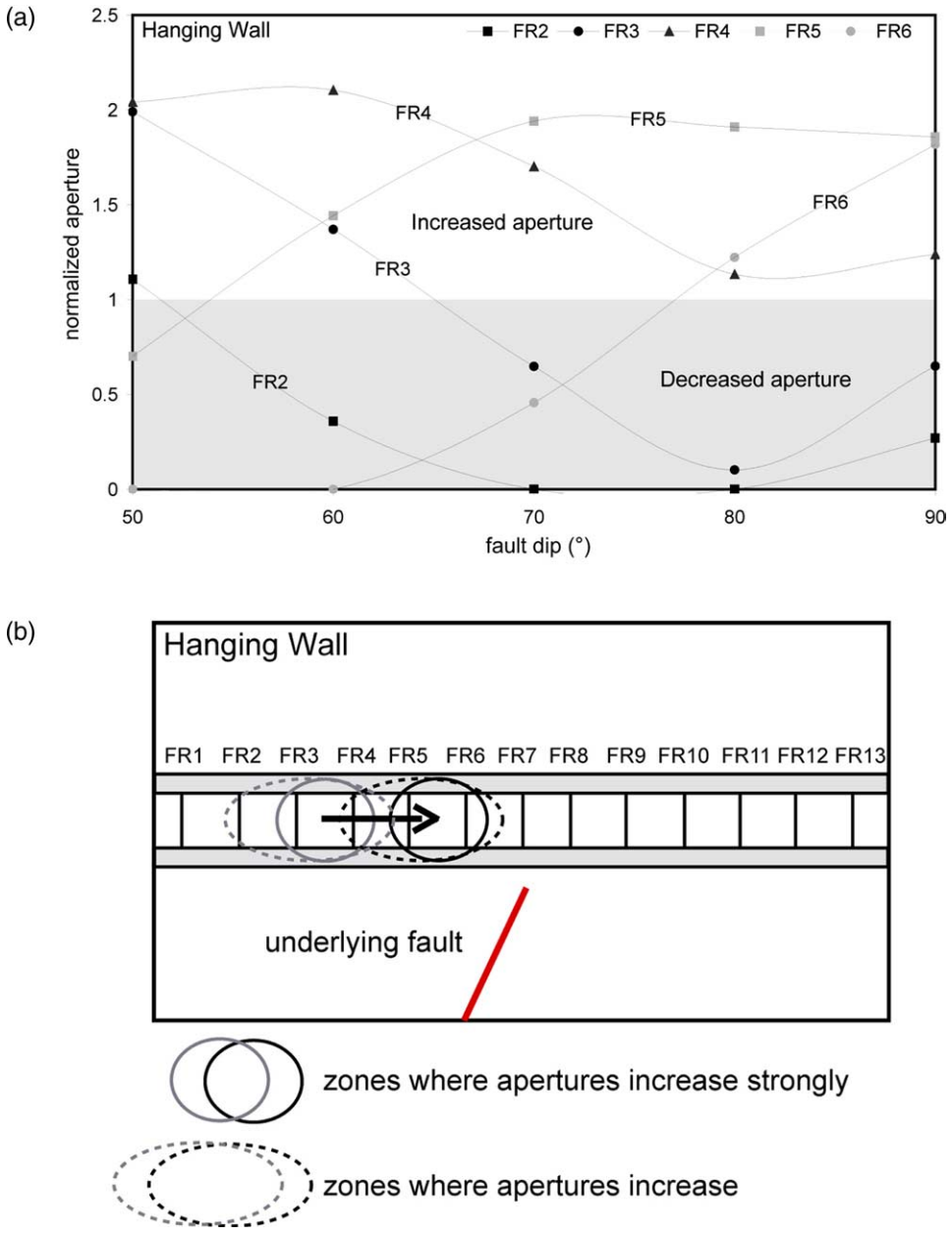

Fig. 4. (a) Evolution in the normalized aperture of fractures FR2–FR6 in the hanging wall of the models as a function of the dip of the underlying fault. The domain corresponding to decreased apertures is shown in grey (same convention used in following figures). (b) Location of the area of increased fracture aperture in the hanging wall, and its lateral displacement when the dip of the underlying fault increases.

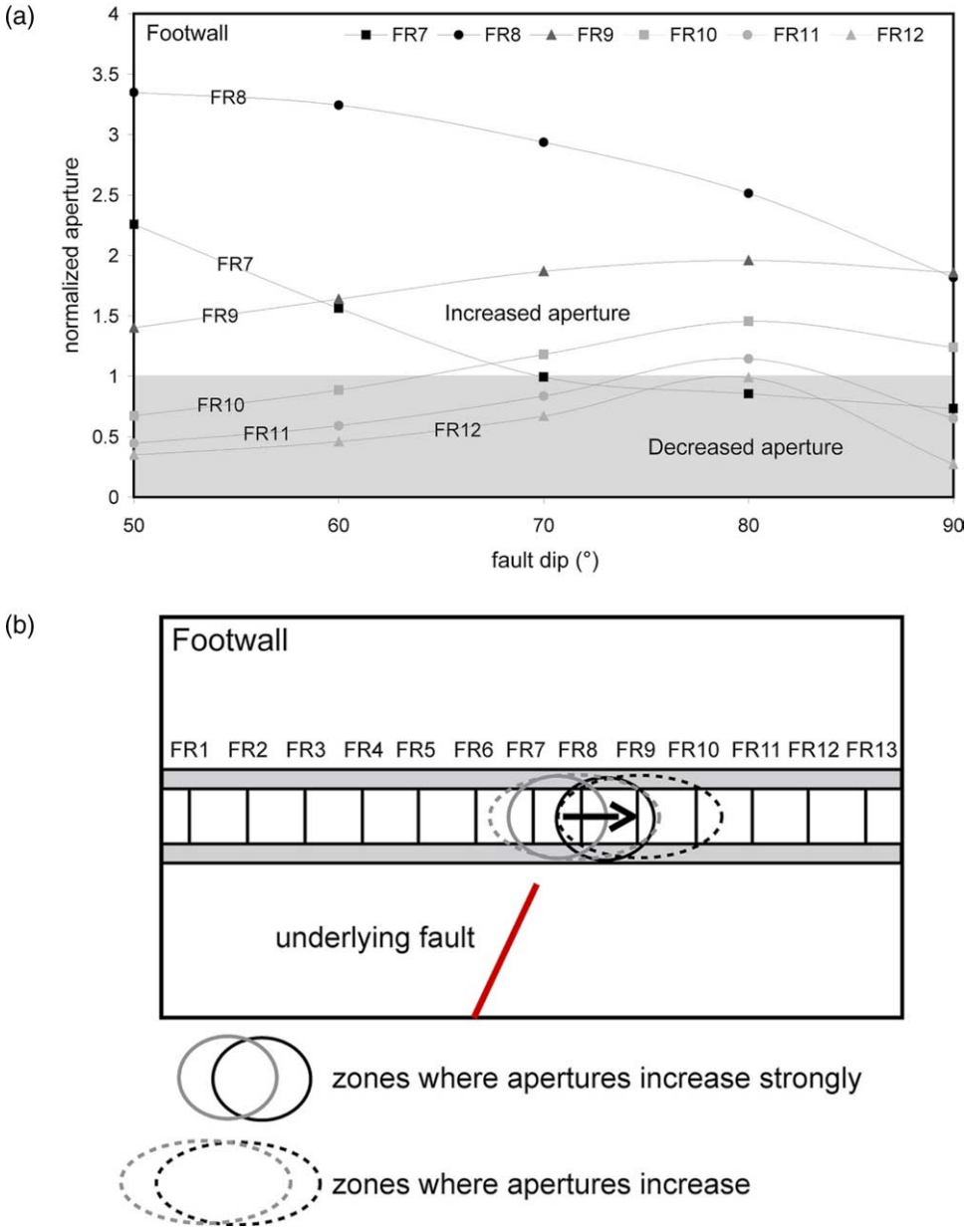

Fig. 5. (a) Evolution in the normalized aperture of fractures FR7–FR12 in the footwall of the models as a function of the dip of the underlying fault. (b) Location of the area of increased fracture aperture in the footwall, and its lateral displacement when the dip of the underlying fault increases.

when the fault dips 50°, this zone is centered on fractures FR3 and FR4, but it moves left to right towards fractures FR5 and FR6 when the dip of the fault increases.

3.1.2. Footwall

Fig. 5a presents the normalized apertures of fractures FR7 to FR12 localized in the footwall of the fault. Fracture FR7, located just above the upper tip of the fault, opens strongly when the fault dips 60° or less, but closes when the fault dip exceeds 70°. Fracture FR8 exhibits the largest increase in aperture with the presence of the underlying fault (its aperture is multiplied by up to 3 when the fault dips 70° or less), but this gain in aperture diminishes continuously when the fault dip increases. The aperture of fracture FR9 is also increased by the presence of the fault, and this gain in aperture increases with the fault dip. Fracture FR10 closes for fault dips smaller than 70° but opens for larger fault dips. Finally, fractures FR11 and FR12 show a similar behavior: they systematically close with the presence of the fault, except when the fault dips 80°, where fracture FR11 exhibits a very limited increase in aperture.

Fig. 5b summarizes these tendencies by showing the location of the area of increased fracture aperture in the footwall: when the fault dips 50°, this zone is centered on fractures FR7 and FR8 but it moves left to right towards fractures FR8 and FR9 when the dip of the fault increases.

3.2. Underlying restraining bends

We now investigate the case of complex fault geometries, where the fault plane consists of several non-parallel segments,

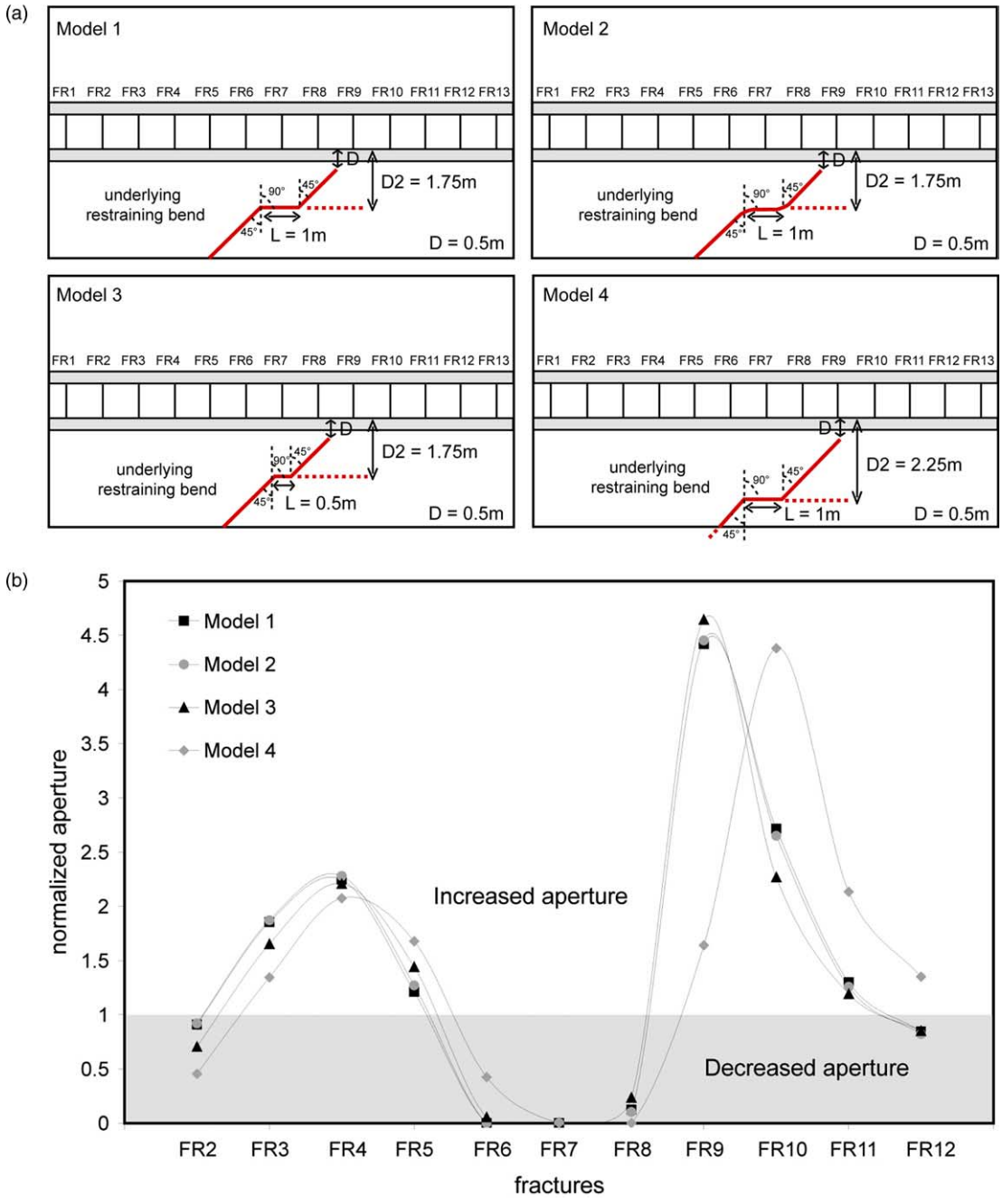

Fig. 6. (a) Geometry of the four models with underlying restraining bends. (b) Normalized fracture apertures in the four models tested.

starting with the situation of restraining bends (Fig. 6a). Four models were tested with different lengths and depths of the horizontal (flat) segment of the fault. Model 2 was created in order to test the effect of smooth fault shapes on fracture aperture.

Fig. 6b presents the evolution in the normalized apertures of fractures FR2–FR12 with the presence of the underlying restraining bends in Models 1–4. It is first shown that the results of Models 1 and 2 are identical, implying that in our models the shape (smooth or sharp) of the underlying fault does not influence the fracture aperture. Second, the four models lead to very similar results. We still observe two zones with increased fracture apertures, one located in the hanging wall and the other located in the footwall; in this second area, the fractures exhibit the greatest increases in aperture: it is multiplied by up to 4.5. Second, fractures FR6–FR8, located right above the flat part of the underlying faults, close completely. The only important difference between the models is that the maximum increase in fracture aperture in the footwall is observed in fracture FR10 for Model 4 and in fracture FR9 for the other models. This is due to the fact that in Model 4, the upper tip of the underlying fault is located between fractures FR9 and FR10 (it was located between fractures FR8 and FR9 in the other models), and Fig. 5a shows that whatever the fault dip, the maximum increase in aperture in the footwall is observed for the fracture located immediately to the right of the upper tip of the fault.

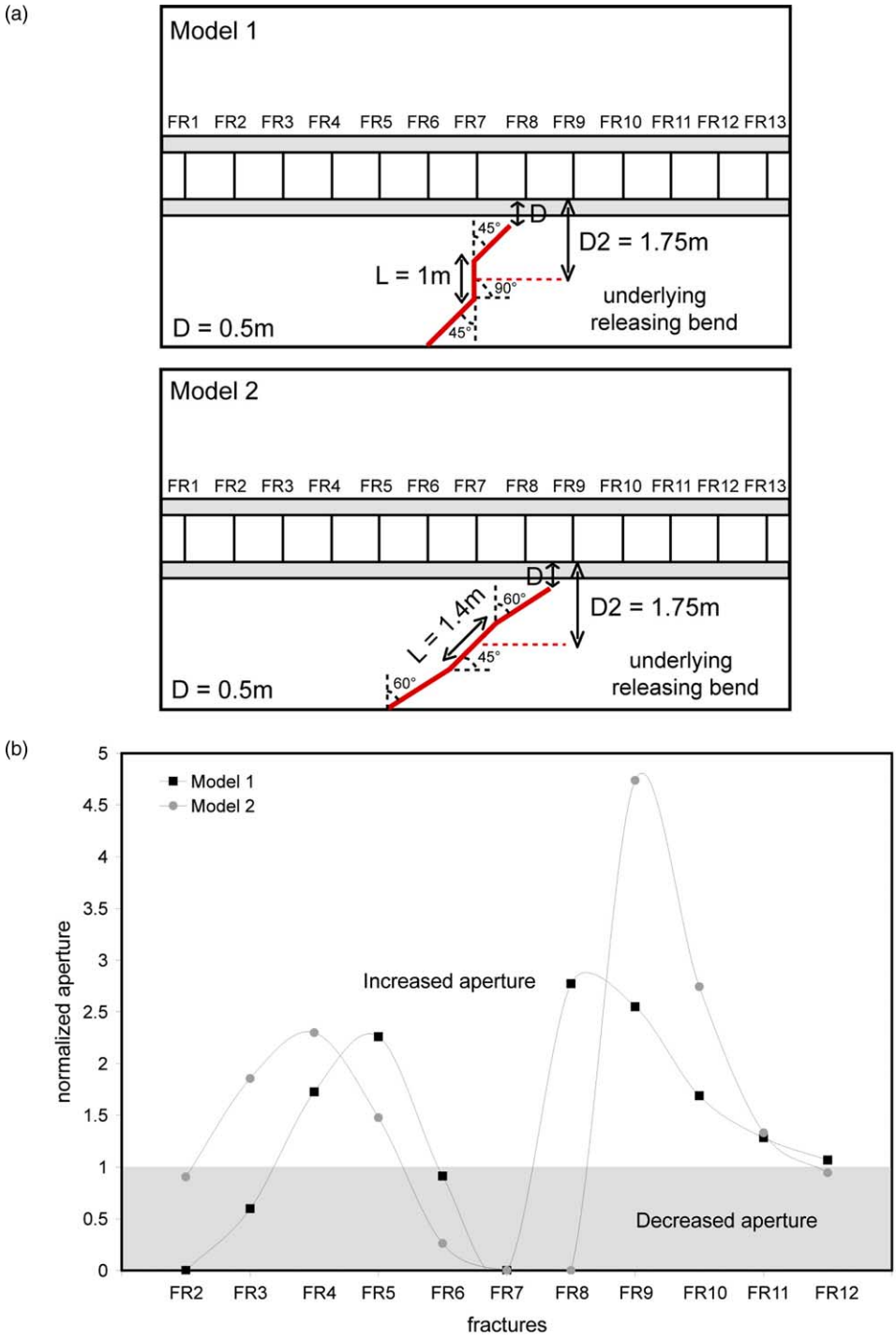

Fig. 7. (a) Geometry of the two models with underlying releasing bends. (b) Normalized fracture apertures in the two models tested.

3.3. Underlying releasing bends

Fig. 7a presents the geometry of the two models of underlying releasing bends tested, which are very different from each other. Fig. 7b presents the evolution in the normalized apertures of fractures FR2–FR12 with the presence of the underlying releasing bends in Models 1 and 2. The results of the two models are similar, and comparable with the previous case of restraining bends. Indeed, the two zones with increased fracture apertures are still observed at the same locations, one in the hanging wall and the other in the footwall. The maximum increase in fracture aperture is larger in the footwall than in the hanging wall. The difference between the two models in the hanging wall is due to the geometry of the zone of changing dip which causes fractures FR6 and FR7 to close strongly to completely in Model 2 while the aperture of fracture FR6 is barely perturbed in Model 1. In the footwall, the difference between the models is in the position of the upper tip of the underlying fault, as it was the case in the previous situation of restraining bends. Finally, we note that when the

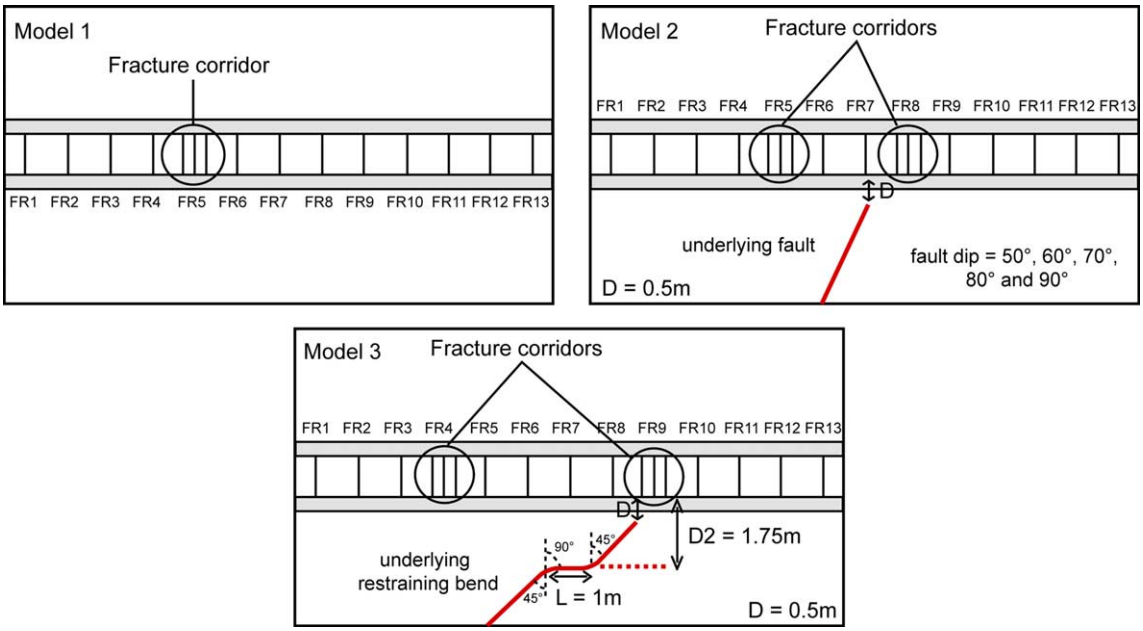

Fig. 8. Geometry and location of the fracture corridors in the three different models tested.

fault presents a high average dip (Model 1), the differences in fracture behavior between the hanging wall and the footwall are less contrasted, and the situation is almost symmetrical.

3.4. Fractures corridors

We now present results concerning fracture corridors formed by three equally spaced fractures. Fig. 8 presents the different models tested. In Models 2 and 3, the fracture corridors were created at the exact location of fractures presenting the greatest increase in aperture due to the presence of the underlying fault. In the tests, we normalized the total aperture of the fracture corridors (= sum of the apertures of the three fractures of the corridors) by dividing it by the aperture of a single fracture located at the same place in an otherwise identical model.

First, we tested the influence of fracture spacing in the corridors, in a model without underlying fault. The results (upper part of Table 1) show that when the fracture spacing in a corridor increases from 0.2 to 0.45 m, the normalized total aperture of the corridor increases from 1.42 to 1.65. As a consequence, in Models 2 and 3 the fracture spacing in the corridors was set to 0.45 m.

Second, we tested the effect of fault dip in the situation of a straight underlying normal fault. It is shown in Table 1 (middle part) that the apertures of the corridors decrease when the fault dip increases. These apertures are slightly larger in the footwall than in the hanging wall, and range from 1.57 to 1.69.

Finally, we addressed the case of an underlying restraining bend. Here, the normalized apertures of the corridors calculated (1.41 and 1.62) are comparable with that of corridors in the previous case of a straight underlying fault but this time the corridor located in the hanging wall is more open. This is due to the fact that the left fracture of the corridor located in the footwall closed completely during the test, because of its close proximity to the upper tip of the underlying fault. As a result it did not contribute to the total aperture of the corridor of the footwall, which was consequently less than the total aperture of the corridor in the hanging wall (composed of three open fractures).

4. Interpretation

In order to interpret the results presented above, we carried out additional experiments to analyze the role of the underlying fault on the distribution of the horizontal tensile stress

Table 1
Normalized aperture of the fractures corridors for each situation investigated.

No underlying fault (Model 1)						
Fracture spacing in the corridor (m)	0.2	0.25	0.3	0.35	0.4	0.45
Normalized aperture of the corridor	1.42	1.46	1.51	1.54	1.6	1.65
Oblique underlying fault (Model 2)						
Dip of underlying fault (°)	50	60	70	80		
Normalized aperture of the corridor (hanging wall)	1.61	1.6	1.57	1.57		
Normalized aperture of the corridor (footwall)	1.69	1.68	1.65	1.62		
Underlying restraining bend (Model 3)						
Normalized aperture of the corridor (hanging wall)	1.62					
Normalized aperture of the corridor (footwall)	1.41					

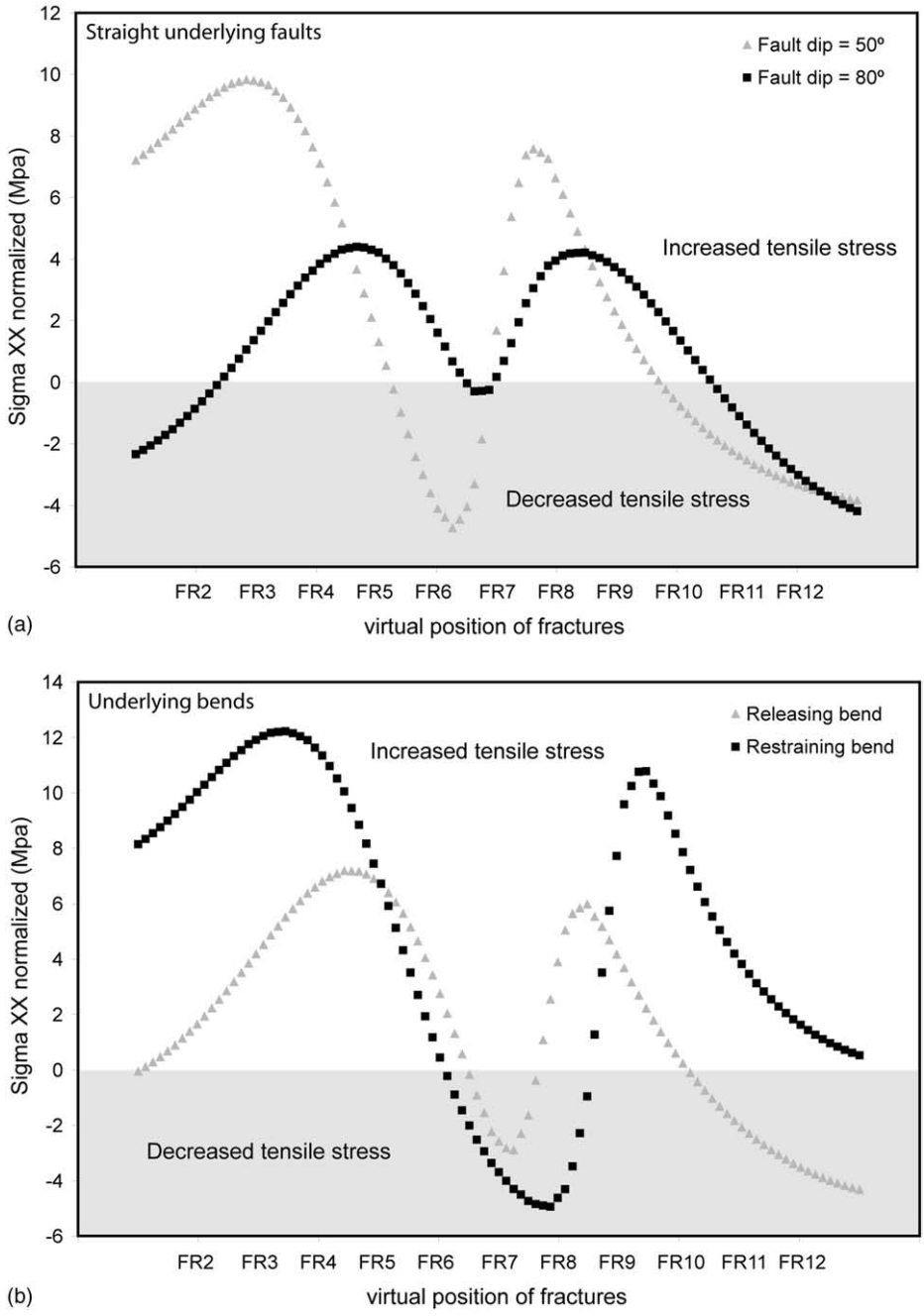

Fig. 9. (a) Normalized horizontal tensile stress (Sigma XX normalized) along a horizontal section in the middle of the central stiff layer of models with straight underlying faults dipping 50 and 80°. (b) Same results in the case of models with restraining/releasing underlying bends (respectively comparable with Model 1 of Fig. 6a and Model 1 of Fig. 7a). The (virtual) position of fractures FR2–FR12 is given to allow the comparison with models containing fractures.

perpendicular to the fractures (Sigma XX) within the central stiff layer. In these experiments, the models present similar geometrical and elastic characteristics to the previous models, but do not contain a row of open fractures in the central stiff layer. Several fault configurations were tested: straight faults dipping 50 and 80°, and models comparable with Model 1 of restraining bend (Fig. 6a) and Model 1 of releasing bend (Fig. 7a). The horizontal (tensile) stress was computed in the models along a horizontal line in the middle of the central stiff layer (i.e. in the location where the fracture apertures were previously calculated). The stress values were normalized (by subtraction) to the stress at the same location in a reference model where neither fault nor fractures are present. Positive values indicate that the presence of the underlying fault results in an increase in tensile stress and negative values indicate a decrease in tensile stress. Fig. 9 presents the results obtained, and shows the virtual position of the fractures present in the previous models. It is shown that the presence of an underlying fault completely redistributes the tensile stress within the central stiff layer. In the case of a straight fault (Fig. 9a), two zones of increased tensile stress are found, one in the hanging wall centered on fractures FR4 or FR5 and the other in the

footwall centered on fractures FR8 or FR9. An increasing dip of the fault results in a lateral displacement of these areas towards the footwall, explaining the tendencies shown by Figs. 4a and 5a. The areas where the tensile stress is increased by the presence of the underlying fault almost exactly superimpose with the areas where the fracture aperture increases in the models containing the fractures. Specifically, Fig. 9a predicts an increase in fracture aperture at the location of fractures FR2–FR5 and FR8–FR10 and a decrease in fracture aperture at the location of fractures FR6 and FR7 (following the fault dip), which almost exactly fits with the results presented by Figs. 4a and 5a. The main difference between the models with and without fractures is that the increases in tensile stress are the largest in the hanging wall in Fig. 9a, whereas the increases in aperture are the largest in the footwall in Figs. 4a and 5a. This difference is due to the fact that the local stress field controlling fracture aperture is not only perturbed by the underlying fault, but also by the fractures themselves, which are absent in the last models studied. However, the results above clearly suggest that the contrasting fracture apertures in the models are mainly related to the modification of the stress field in the central stiff layer due to the presence of the underlying fault.

Concerning the bend configurations (Fig. 9b), the tendencies shown in terms of tensile stress modifications due to the underlying fault are comparable between the releasing and restraining bends. The horizontal tensile stress decreases at the location of fractures FR6–FR8, and increases at the location of fractures FR2–FR5 in the hanging wall and at the location of fractures FR8–FR12 in the footwall (following the models). We note that these results are very close to those of Figs. 6b and 7b in terms of fracture aperture. For example, Fig. 9b shows a maximum increase in tensile stress near location of fractures FR4 and FR9, and these fractures are the ones exhibiting the largest increase in aperture in Fig. 6b. Nevertheless, once again, the increases in horizontal tensile stress are the largest in the hanging wall in Fig. 9b, whereas the increases in aperture are the largest in the footwall in Figs. 6b and 7b.

In the case of the straight underlying fault, the zones of increased tensile stress (Fig. 9a) and the zones of increased fracture apertures (Figs. 4 and 5) move left to right towards the footwall when the fault dip increases. We are aware that this direction of movement is somewhat counterintuitive compared with the well known case of a mode II sliding crack in a homogeneous material. In the latter situation, the lobe of tensile stress at the tip of the crack would rotate counter-clockwise (and would move right to left and towards the hanging wall) with an increasing dip of the crack. The explanation to this apparent inconsistency is that the soft layers

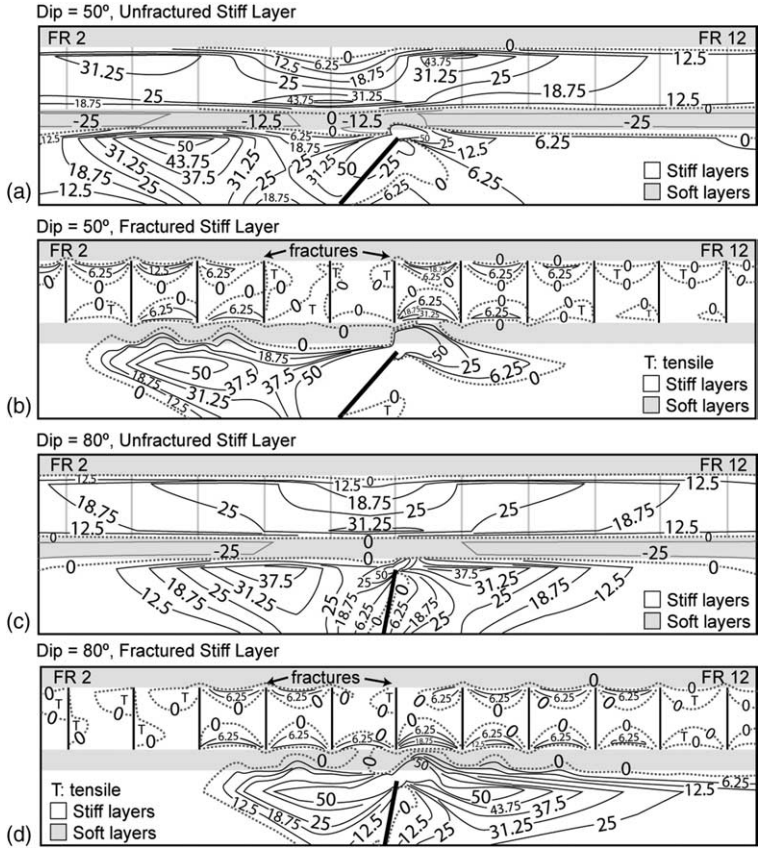

Fig. 10. Contour plots of the horizontal stress Sigma XX in models with straight underlying faults (stress contours in Mpa, limits of the figures are not the limits of the models). T indicates tensile stress areas when not obvious. Dashed lines are contours marking the limits between tensile (positive) and compressive (negative) stress. True (black) or virtual (grey) fractures are drawn in the central stiff layer, and FR2 and FR12 indicate the positions of the two fractures at the extremities of the fracture row. (a) Model with a straight underlying fault dipping 50° and no fractures. (b) Same model as in (a) with fractures in the central stiff layer. (c) Model with a straight underlying fault dipping 80° and no fractures. (d) Same model as in (c) with fractures in the central stiff layer.

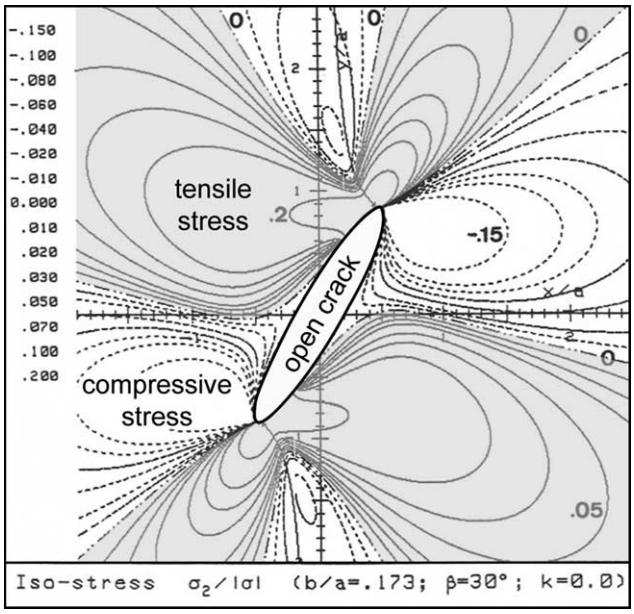

Fig. 11. Analytical contour plots of the normalized minor principal stress σ_2 around an elliptical open crack oriented at 30° with the vertical compression. The zones of tensile stress are highlighted in grey (modified from M. Barquins, personal communication).

play a role in distorting the stress field near the fault tip in our models. As shown by Fig. 10a and c, the soft layer directly above the fault tip perturbs the growth of the lobe of tensile stress at the tip of the fault. This lobe cannot develop towards the soft layer, which is a zone of compressive stress acting as a barrier between the fault tip and the central stiff layer. Fig. 11 shows the lobes of tensile stress at the tips of a mode II elliptical crack in a homogeneous material for comparison. In this situation, the lobes of tensile stress are well developed and extend far away from the crack tips, which is not possible in our models because of the presence of the soft layer.

In Fig. 10a and c, the stress field in the central stiff layer is influenced by the combined effects of the fault and the soft layers in response to the applied deformation: when the fault dip increases from 50 to 80°, the zones of maximum tensile stress in the middle of the layer move left to right in the hanging wall and the footwall. In the models with fractures (Fig. 10b and d), the stress field is more perturbed, particularly in the fractured layer. The presence of fractures with spacing equal to the height of the layer prevents the development of large areas of tensile stress in the middle of the layer, as described in Bai and Pollard (2000b). The fractures exhibiting increased aperture are the fractures between which continuous lobes of tensile stress develop near or at the two interfaces with the surrounding soft layers (fractures FR2–FR4 and FR7–FR9, Fig. 10b; fractures FR4–FR6 and FR8–FR11, Fig. 10d). When the dip of the fault increases, the zones with well developed tensile lobes between the fractures move left to right in the hanging wall and extend to the right in the footwall, explaining the tendencies shown by Figs. 4, 5 and 9a.

Finally, it was shown that the aperture of a fracture corridor composed of three equally spaced fractures always ranges from 1.41 to 1.69 times the aperture of a single fracture, whatever the situation investigated. The reason for such similar increases in aperture within the corridors lies in the behavior of the three fractures composing the corridors. Due to their spacing, which is smaller than that of the original fractures in the models, these three fractures cannot open as much as the individual fractures. The two external fractures of the corridors showed apertures generally equal to 60–70% of the aperture of individual fractures located in the same area, and the central fracture was shown to be perturbed by its two close neighbors, and to contribute by less than 20% to the total aperture of the corridor. These central fractures exhibited apertures equal to less than 30% of the aperture of individual fractures located in the same area, limiting the increase in aperture represented by the corridors with respect to the case of single fractures.

5. Discussion

We now discuss the possible application of the results presented above.

First, we considered the mechanical behavior of fractures with perfectly smooth surfaces. However, in nature, fractures always present a certain roughness, which may correspond to the fractographic features inherited from their propagation under mode I conditions (Bahat, 1991; Auzias et al., 1993). When important, this fracture roughness may imply an interlocking behavior between asperities on the two opposite surfaces of the fractures. In this situation, one can expect that the eventual increase or decrease in fracture aperture due to the presence of an underlying fault would be reduced with respect to our experiments. The fractures would not be able to open or close as freely as in our models, due to friction at the contact between the asperities. However, our results may be applicable to the behavior of natural fractures with a moderate roughness and no interlocking, which is not expected to be very different from that of the 'flat' fractures in our experiments. Furthermore, fracture roughness has been shown to play an important role in fracture permeability in the case of small fracture apertures (Brown, 1989). In these conditions, it would be premature to directly extend our results in terms of fracture aperture to possible fracture permeability, especially in the situation of natural fractures with low initial aperture.

Second, the fracture behaviors described in our models are mainly related to the local stress perturbations around the upper tip of the underlying fault (see the interpretation of the results above). In the experiments, the underlying faults were frictionless, leading to strong stress perturbations. In these conditions, one can wonder how our results compare with the case of natural faults sliding with friction. The friction significantly reduces the displacement along the faults with respect to the frictionless situation, leading to a reduction of the stress perturbations at the fault tips. However, evidence of significant stress perturbations near the tips of faults sliding with friction can be found in the literature. Numerous examples of Mode I fractures developing at the tips of natural faults have been described (Segall and Pollard, 1983; Granier, 1985; Petit, 1987), accounting for important tensile stress concentrations, and pressure solutions have been shown to develop at fault tips

due to significant compressive stress concentrations (Rispoli, 1981; Petit and Mattauer, 1995). Therefore, the fracture behaviors (opening/closing) described in this study may still apply in the case of natural fractures located above a fault sliding with friction, even if a reduced stress perturbation at the fault tips would lead to less distinct fracture behaviors. Nevertheless, in nature, friction may be reduced by the presence of clay-rich core zones, or by abnormal fluid pressure.

Third, while we considered changes in the 2D (cross-section) geometry of the faults in our models, natural faults also display changes in their along-strike geometry. The along-strike segmentation of faults may have an important influence on the behavior of the fractures in the overlying layers. As discussed in a previous section, the opening/closing tendencies shown by the fractures in our models are mainly related to stress perturbations at the tips of the underlying faults. In these conditions, we expect the zones of increased/decreased fracture aperture to be found at the same locations all along (above) a given fault segment in the along-strike direction, because the stress perturbations are not expected to vary greatly along a continuous segment. However, in the relay zones between consecutive fault segments, the stress perturbations are dramatically increased due to the interaction of several fault tips. These intense stress perturbations would probably result in extreme fracture behaviors when compared with the situation in our models. In fault relay zones, we would expect fractures to either completely close or demonstrate very large apertures depending on their location with respect to the segment tips. Furthermore, fault relay zones are densely fractured, which may facilitate the circulation of fluids towards the overlying layers and thus increase the volume of fluids drained by the open fractures above units.

Even if we are aware of the potential limitations of this work, the distinct tendencies in terms of fracture aperture that we described provide a satisfying explanation to localized flow through a joint set in a well-defined layer as shown in Bruel et al. (1999). These authors observed very localized water flow through a few bed-limited adjacent joints at depth in an uranium mine in the Lodève Permian Basin (Southern France), with the neighboring joints (with identical aspect) being dry. The presence of an unconnected and non-observable fault, redistributing the local elastic stress field in layers apparently unaffected by deformation and enhancing fracture apertures very locally, may be responsible for such discontinuous flow in a systematic joint set.

Finally, the increase in aperture due to the presence of fracture corridors in the models strongly suggests their possible role as preferential geological drains. These corridors, commonly observed in many geological contexts and sometimes composed of many tens of fractures, may act as high permeability conduits in oil and gas reservoirs.

6. Conclusions

This work is a 2D numerical contribution to the problem of fault and fracture interaction in rocks, focusing on the modification in fracture aperture induced by the presence of an underlying unconnected normal fault. First, it is shown that the presence of an underlying fault strongly affects the aperture of the fractures above, leading to much contrasted situations. The fractures situated near the tip of the fault in two very local areas, one in the hanging wall and the other in the footwall, exhibit increased aperture, whereas the neighboring fractures tend to close. The increases in aperture are systematically greater in the footwall than in the hanging wall, and the zones with increased fracture aperture move towards the footwall when the fault dip increases. Second, the fracture behaviors described in the case of a straight underlying fault are still observed in the case of underlying restraining/releasing bends. Nevertheless, if the gains in fracture aperture are comparable with the case of the straight fault in the hanging wall, they increase strongly in the footwall. The particular distribution of areas where the fracture aperture is enhanced, which can be superimposed to the areas where the horizontal tensile stress is increased by the presence of the underlying fault, may have an application to the observed heterogeneous fluid flow through joint sets.

Finally, the case of fracture corridors is addressed. It is shown that, whatever the characteristics of the underlying fault, the total aperture of a corridor of three fractures is equal to 1.41–1.69 times the aperture of a single fracture located at the same place in the fractured layer. This strongly suggests their possible role as preferential geological drains, with hydrodynamical consequences on fluid flow in oil and gas reservoirs.

Acknowledgements

This work is part of Ghislain de Joussineau's PhD thesis, funded by the French Research Ministry. We acknowledge the thoughtful reviews by David Healy, Terry Engelder and Jonathan Imber. We warmly thank Joseph Gonzales for a revision of the English of the manuscript. Finally, we are grateful to the Cornell Fracture Group for free use of Franc 2D and technical help.

References

Antonellini, M., Aydin, A., 1994. Effect of faulting on fluid flow in porous sandstones: petrophysical properties. American Association of Petroleum Geologists Bulletin 78, 355–377.

Atkinson, B.K., 1987. Fracture Mechanics of Rocks. Academic Press, London.

Auzias, V., Rives, T., Petit, J.P., 1993. Signification des côtes (rib marks) dans la cinétique de propagation des diaclases: modèle analogique dans le polyméthacrylate de méthyle (PMMA). Comptes Rendus de l'Académie des Sciences de Paris série II 317, 705–712.

Aydin, A., 2000. Fractures, faults, and hydrocarbon entrapment, migration and flow. Marine and Petroleum Geology 17, 797–814.

Bahat, D., 1991. Tectono-fractography. Springer-Verlag, Berlin.

Bai, T., Pollard, D.D., 2000a. Fracture spacing in layered rocks: a new explanation based on the stress transition. Journal of Structural Geology 22, 43–57.

Bai, T., Pollard, D.D., 2000b. Closely spaced fractures in layered rocks: initiation mechanism and propagation kinematics. Journal of Structural Geology 22, 1409–1425.

Bai, T., Pollard, D.D., Gao, H., 2000a. Explanation for fracture spacing in layered materials. Nature 403, 753–756.

Bai, T., Pollard, D.D., Gross, M., 2000b. Mechanical prediction of fracture aperture in layered rocks. Journal of Geophysical Research 105, 707–721.

Bai, T., Pollard, D.D., 2001. Getting more for less: the unusual efficiency of fluid flow in fractures. Geophysical Research Letters 28, 65–68.

Brown, S.R., 1989. Transport of fluid and electric current through a single fracture. Journal of Geophysical Research 94, 9429–9438.

Bruel, T., Petit, J.P., Massonnat, G., Guerin, R., Nolf, J.L., 1999. Relation entre écoulements et fractures ouvertes dans un système aquifère compartimenté par des failles et mise en évidence d'une double porosité de fractures. Bulletin de la Société Géologique de France 170-3, 401–412.

Cacas, M.C., Ledoux, E., de Marsily, G., Tillie, B., 1990. Modeling fracture flow with a stochastic discrete fracture network; calibration and validation. Water Resources Research 26, 479–489.

Connolly, P., 1999. The Fracture Corridor Project, Part 1. Technical Report. Elf Aquitaine-Shell International Exploration & Production B.V..

de Joussineau, G., 2003. Contribution à l'étude du comportement sous contrainte des failles et des fractures de mode I: terrain, et modélisations analogiques et numériques. PhD Thesis, Université Montpellier II.

de Joussineau, G., 2003b. 2D Numerical Investigation of the Mechanics of Jointing Within Layered Rocks: Towards the Origin of Fracture Corridors. Technicol Report. Shell International Exploration & Production.

Eichhulb, P., Taylor, W.L., Pollard, D.D., Aydin, A., 2004. Paleo-fluid flow and deformation in the Aztec Sandstone at the Valley of Fire, Nevada—evidence for the coupling of hydrogeologic, diagenetic and tectonic processes. Geological Society of America Bulletin 116, 1120–1136.

Engelder, T., Peacock, D.C.P., 2001. Joint development normal to regional compression during flexural-flow folding: the Lilstock buttress anticline, Somerset, England. Journal of Structural Geology 23, 259–277.

Fisher, M.P., Gross, M.R., Engelder, T., Greenfield, R.J., 1995. Finite-element analysis of the stress distribution around a pressurized crack in a layered elastic medium: implications for the spacing of fluid-driven joints in bedded sedimentary rocks. Tectonophysics 247, 49–64.

Granier, T., 1985. Origin, damping, and pattern of development of faults in granite. Tectonics 4, 721–737.

Gringarten, E., 1996. 3-D geometric description of fractured reservoirs. Mathematical Geology 28, 881–893.

Gross, M.R., Fisher, M.P., Engelder, T., Greenfield, R.J., 1995. Factors controlling joint spacing in interbedded sedimentary rocks: integrating numerical models with field observations from the Monterey Formation, USA. In: Ameen, M.S. (Ed.), Fracture Topography as a Tool in Fracture Mechanics and Stress Analysis Geological Society Special Publications 92, pp. 215–233.

McConaughy, D.T., Engelder, T., 2001. Joint initiation in bedded clastic rocks. Journal of Structural Geology 23, 203–221.

Nordqvist, A.W., Tsang, Y.W., Tsang, C.F., Dverstorp, B., Andersson, J., 1992. A variable aperture fracture network model for flow and transport in fractured rocks. Water Resources Research 28, 1703–1713.

Oda, M., 1986. An equivalent continuum model for coupled stress and fluid flow analysis in jointed rock masses. Water Resources Research 22, 1845–1856.

Petit, J.P., 1987. Criteria for the sense of movement on fault surfaces in brittle rocks. Journal of Structural Geology 9, 597–608.

Petit, J.P., Barquins, M., 1988. Can natural faults propagate under mode II conditions? Tectonics 7, 1243–1256.

Petit, J.P., Mattauer, M., 1995. Paleostress superimposition deduced from mesoscale structures in limestone: the Matelles exposure, Languedoc, France. Journal of Structural Geology 2, 245–256.

Petit, J.P., Bazalgette, L., Chemenda, A., Connolly, P., Jorand, C., de Joussineau, G., 2004. Fracture corridors. Fractured Reservoirs Conference, The Geological Society of London, November 16–17, London.

Pollard, D.D., Segall, P., 1987. Theoretical displacements and stresses near fractures in rock: with applications to faults, joints, veins, dikes, and solution surfaces. In: Atkinson, B.K. (Ed.), Fracture Mechanics of Rocks. Academic Press, London, pp. 277–349.

Pyrak-Nolte, L.J., Cook, N.G.W., Nolte, D.D., 1988. Fluid percolation through single fractures. Geophysical Research Letters 15, 1247–1250.

Renshaw, C.E., 1995. On the relationship between mechanical and hydraulic apertures in rough-walled fractures. Journal of Geophysical Research 100, 24629–24636.

Rispoli, R., 1981. Stress field about strike-slip faults inferred from stylolites and tension gashes. Tectonophysics 75, 29–36.

Segall, P., Pollard, D.D., 1983. Nucleation and growth of strike-slip faults in granite. Journal of Geophysical Research 88, 555–568.

Wawrzynek, P.A., Ingraffea, A.R., 1987. Interactive finite element analysis of fracture processes: an integrated approach. Theoretical and Applied Fracture Mechanics 8, 137–150.